*Biochemical Journal* (2017) **474** 3485–3498
DOI: 10.1042/BCJ20170515

PORTLAND PRESS

Research Article

# Bindings of NO, CO, and $O_2$ to multifunctional globin type dehaloperoxidase follow the 'sliding scale rule'

**Gang Wu[1], Jing Zhao[2], Stefan Franzen[2] and Ah-Lim Tsai[1]**

[1]Division of Hematology, Department of Internal Medicine, The University of Texas Health Science Center at Houston — McGovern Medical School, Houston, TX 77030, U.S.A.; [2]Department of Chemistry, North Carolina State University, Raleigh, NC 27695, U.S.A.

**Correspondence:** Stefan Franzen (franzen@ncsu.edu) or Ah-Lim Tsai (ah-lim.tsai@uth.tmc.edu)

Dehaloperoxidase–hemoglobin (DHP), a multifunctional globin protein, not only functions as an oxygen carrier as typical globins such as myoglobin and hemoglobin, but also as a peroxidase, a mono- and dioxygenase, peroxygenase, and an oxidase. Kinetics of DHP binding to NO, CO, and $O_2$ were characterized for wild-type DHP A and B and the H55D and H55V DHP A mutants using stopped-flow methods. All three gaseous ligands bind to DHP significantly more weakly than sperm whale myoglobin (SWMb). Both CO and NO bind to DHP in a one-step process to form a stable six-coordinate complex. Multiple-step NO binding is not observed in DHP, which is similar to observations in SWMb, but in contrast with many heme sensor proteins. The weak affinity of DHP for $O_2$ is mainly due to a fast $O_2$ dissociation rate, in accordance with a longer $^{\varepsilon}$N–Fe distance between the heme iron and distal histidine in DHP than that in Mb, and an open-distal pocket that permits ligand escape. Binding affinities in DHP show the same 3–4 orders separation between the pairs NO/CO and CO/$O_2$, consistent with the 'sliding scale rule' hypothesis. Strong gaseous ligand discrimination by DHP is very different from that observed in typical peroxidases, which show poor gaseous ligand selectivity, correlating with a neutral proximal imidazole ligand rather than an imidazolate. The present study provides useful insights into the rationale for DHP to function both as mono-oxygenase and oxidase, and is the first example of a globin peroxidase shown to follow the 'sliding scale rule' hypothesis in gaseous ligand discrimination.

## Introduction

Dehaloperoxidase–hemoglobin (DHP) is a heme-containing globin, which accounts for ∼3% the soluble protein in crude extracts of the terebellid polychaete *Amphitrite ornata* (*A. ornata*) [1]. DHP has two forms, DHP A and B, which are coded by different genes and distinguished by five amino acids in the peptide sequences [2]. In its environment in a tube buried in shallow coastal mudflats and estuaries, *A. ornata* is known to use DHP as a primary enzyme for detoxification of naturally occurring toxins, including brominated phenols, indoles, and pyrroles among other halogenated aromatic hydrocarbons. Both DHP isozymes exhibit peroxidase activity, catalytically dehalogenating trihalophenols, which are widely found in benthic ecosystems to dihaloquinones in the presence of co-substrate $H_2O_2$ [1,3,4]. The phenols are potentially toxic to sediment-dwelling invertebrates due to their tendency to react to form dioxins and other reactive molecules that can interfere with replication. The quinone products of the DHP peroxidation reactions are much less harmful to *A. ornata*. More recently, DHP has been shown to exhibit peroxygenase and oxidase activities toward a range of substrates including dibromophenols, brominated indoles, and pyrroles [5,6]. Isolated DHP isozymes are also shown to have oxygen storage/transfer capabilities, which are consistent with their abundance in

Received: 28 June 2017
Revised: 6 September 2017
Accepted: 12 September 2017

Accepted Manuscript online: 12 September 2017
Version of Record published: 5 October 2017

Biochemical Journal (2017) **474** 3485–3498
DOI: 10.1042/BCJ20170515

the coelom of *A. ornata*. DHP A and B are also both present in erythrocruorin, the giant hemoglobin (Hb) in the small tentacles of *A. ornata* that are usually visible above the surface of mudflat, where the organism is resident [5]. Both the abundance of DHP in the coelom and the existence of erythrocruorin strongly suggest that DHP is the principal protein responsible for oxygen transport and storage in *A. ornata* as well.

The peroxidase activity of DHP apparently contradicts its identity as a globin. Peroxidases are known to activate O–O bond cleavage of bound $H_2O_2$ while globins have a primary function to reversibly bind $O_2$. Peroxidases normally have a ferric resting state while globins have a ferrous resting state. The functional differences between peroxidases and globins would seem to be so great that the idea of globin peroxidase seems like a contradiction. The resolution of this contradiction starts with the measurement of the high redox potential of 221 mV for DHP [7,8]. This redox potential is 100–150 mV higher than the average values of globins, stabilizing ferrous heme and supporting the oxygen storage/transport function observed in myoglobin (Mb) and Hb. The shift in redox potential in DHP is opposite to that of typical peroxidases, which are more negative by ~250–300 mV relative to the globins. The negative redox potentials support stable ferric resting states in typical peroxidases [9]. The apparently paradoxical dual functions of DHP can be explained in part by a hypothesis that the peroxidation cycle is shifted, which means that it goes from the oxyferrous state directly to compound II (instead from the ferric state to compound I) when $H_2O_2$ binds. The flexibility of the distal histidine (His55) appears to have evolved to play a crucial role in $H_2O_2$ binding in the ferrous form of DHP. There is evidence that His55 exists in multiple conformations. In the first conformation (globin form), His55 stabilizes the Fe(II)–$O_2$ species, but then switches to a different conformation enforced by substrate binding to facilitate the deprotonation of $H_2O_2$ and subsequent heterolytic O–O bond cleavage in the peroxidase cycle [5,10,11]. Consistent with the functional switch, the $N^{\varepsilon}$–Fe distance in DHP (5.4–5.5 Å) [12] is intermediate between that of horseradish peroxidase (HRP, 6.0 Å) and Mb (4.3–4.5 Å) [13–15]. The dynamics of His55, switching between the 'open' (inactive) and 'closed' (active) conformations, is proposed to be regulated by the binding of mono- and trihalophenol substrates, respectively [16,17].

In its peroxidase reactions, DHP has been proposed to react with $H_2O_2$ in its Fe(III), Fe(II), and even Fe(II)–$O_2$ states to generate Compound I, Complex ES, and Compound II high oxidation state intermediates [5,10,18–20]. These intermediates can be cycled back to either Fe(II) or Fe(III) heme by various halophenol co-substrates or their secondary products, or by some yet to be identified source(s) of reducing equivalents, facilitated by the intrinsic high midpoint potentials of the Fe(IV)/Fe(III) and Fe(III)/Fe(II) half reactions [5]. The versatility of DHP in catalysis is further demonstrated by peroxygenase and oxidase reactivities using haloindoles and nitrophenols as substrates, confirmed by $^{18}O$-labeled co-substrate analogs [21,22]. Moreover, isolated DHP is recently reported to exhibit P450 like mono-oxygenase and lipoxygenase-like dioxygenase activities using 5,5′-dibromo-indigo and 2,3-dimethylindole as co-substrates, respectively [23].

In addition to the uncommon multifunctional enzymatic activities, the other important aspect of multifunctional DHP is its oxygen storage/transfer function. To understand the oxygen storage/transfer function of DHP, a careful characterization of its binding to oxygen is essential. The oxygen dissociation constant of DHP, $K_D(O_2)$, was recently measured: 7.7 μM for DHP A and about half of this value for DHP B [24], both about one order of magnitude weaker than that of sperm whale Mb (SWMb) [25–27]. However, the method used for the $K_D(O_2)$ measurement is based on a competition binding assay with *t*-butyl isocyanide and does not provide any kinetic information for $O_2$ binding. Direct monitoring of the $O_2$ reaction with DHP should reveal the kinetics/affinity of $O_2$ binding to DHP. The binding kinetics/affinity of DHP for other gaseous ligands, NO and CO, can also be measured by directly monitoring their reactions with DHP. These measurements provide insights into whether DHP binds NO, CO, and $O_2$ selectively and may reveal other, as yet unknown, function(s) of DHP.

The 'sliding scale rule' hypothesis, recently derived from bioinformatic graphical analyses based on a large database of hemeproteins containing a five-coordinate (5c) heme ligated to a proximal neutral imidazole, elucidates the 3–4 orders of difference in the affinities of these hemeproteins for the NO/CO and CO/$O_2$ pairs [28,29]. One prominent example is the explanation for one of the most intriguing issues in the gaseous ligand selectivity of mammalian NO sensor soluble guanylyl cyclase (sGC): why sGC is able to bind NO with an apparent $K_D$ of pM but totally exclude $O_2$ [29]. On the other hand, typical peroxidases, such as HRP and cytochrome *c* peroxidase (CCP), which commonly have an imidazolate proximal heme ligand, exhibit very poor gaseous ligand selectivity due to the high-ligand field strength. Given this background, it is of interest to examine whether DHP, as an unusual peroxidase, is capable of selectively binding NO, CO, and $O_2$.

Biochemical Journal (2017) **474** 3485–3498
DOI: 10.1042/BCJ20170515

In the present study, we conducted systematic kinetic binding measurements of all three gaseous ligands with the multifunctional DHP A and B, and specific His55 mutants of DHP A. The measured kinetic/affinity parameters were subjected to bioinformatic graphical analysis. Both DHP A and B bind NO, CO, and $O_2$ selectively and their $K_D$s for the gaseous ligands follow the 'sliding scale rule'. On the other hand, the data obtained for His55 mutants of DHP A clearly showed the effect of the distal histidine in regulating selectively the $O_2$ binding via specific H-bonding with $O_2$ ligand.

# Experimental

## Materials

All chemicals were purchased from Sigma–Aldrich (St. Louis, MO) and Fisher Scientific (Hampton, NH) and used without further purification. The E.Z.N.A plasmid DNA mini kit was from Omega Bio-Tek (Norcross, GA). The QuikChange II site-directed mutagenesis kit was purchased from Agilent Technologies (Santa Clara, CA). The designed oligonucleotide primers were synthesized by Integrated DNA Technologies (Coralville, IA). CO and NO gases were from Matheson-TriGas, Inc. (Houston, TX). NO was pre-purified by passing through a NaOH trap to remove nitrous and nitric acid contaminants.

## Site-directed mutagenesis and protein purification

DHP A mutations were generated with the QuikChange II site-directed mutagenesis kit using the plasmids encoding wild-type DHP A (wt DHP A with a tag of six histidines at N-terminus) as the templates, and the primers used are listed in Table 1 with mutation sites underlined. The plasmids with the mutations were extracted using a E.Z.N.A plasmid DNA mini kit from the transformed BL21(DE3) *Escherichia coli*, and their integrities were verified by sequencing (Genewiz, South Plainfield, NJ).

WT DHP A, wt DHP B, H55D, and H55V DHP A were expressed and purified as previously described [3]. Briefly, *E. coli* cell pellets were suspended and lysed in the lysis buffer for 4 h. The cell slurry was then centrifuged at 28 000×***g*** for 30 min, and the supernatant was applied to an Ni–NTA column. The protein was eluted, concentrated, and oxidized by $K_3[Fe(CN)_6]$. Unreacted $K_3[Fe(CN)_6]$ was removed by a NAP-25 size exclusion column, and the buffer was simultaneously exchanged into 20 mM potassium phosphate (pH 6). Ferric DHP was then loaded onto a CM-52 ion exchange column and eluted with 150 mM potassium phosphate (pH 7). The concentrations of the purified ferric proteins were determined using the Soret extinction coefficients: wt DHP A and B both with $\varepsilon_{406\ nm} = 116\,400\ M^{-1}\ cm^{-1}$, H55D DHP A with $\varepsilon_{398\ nm} = 82\,500\ M^{-1}\ cm^{-1}$, and H55V DHP A with $\varepsilon_{394\ nm} = 121\,300\ M^{-1}\ cm^{-1}$, respectively. The extinction coefficients of Soret bands of H55D and H55V DHP A were determined via quantification of the heme content by the pyridine hemochrome method [30].

## Measurements of gaseous ligand bindings

The association and dissociation kinetics of NO, CO, and $O_2$ to ferrous DHP were studied with an Applied PhotoPhysics SX-18MV stopped-flow instrument (Leatherhead, U.K.), with its sample handling unit kept in an anaerobic chamber (COY Lab Products, Grass Lake, MI). The anaerobic chamber was filled with a $H_2/N_2$ mixture (typically 7–10% $H_2$) and any residual $O_2$ was removed by reaction with $H_2$ catalyzed by a platinum catalyst. The anaerobic condition in the chamber was indicated by the constant 0 ppm [$O_2$] reading of the $O_2$ meter placed inside the chamber. DHP was reduced by anaerobic $Na_2S_2O_4$ titration in a tonometer after five alternating cycles of vacuum and argon displacement. The CO or NO stock solutions were prepared by long-time flushing of anaerobic buffer with CO or NO gas, respectively.

**Table 1 DNA sequences of primers for DHP A mutant constructs**

| Primer | Sequence |
|---|---|
| H55D forward | 5′- GGCCAAGTTCGGTGATGACACTGAGAAAGTGTTCAACC-3′ |
| H55D reverse | 5′- GGTTGAACACTTTCTCAGTGTCATCACCGAACTTGGCC-3′ |
| H55V forward | 5′-GGCCAAGTTCGGTGATGTTACTGAGAAAGTGTTCAACC-3′ |
| H55V reverse | 5′-GGTTGAACACTTTCTCAGTAACATCACCGAACTTGGCC-3′ |

Biochemical Journal (2017) 474 3485–3498
DOI: 10.1042/BCJ20170515

The time courses of different wavelengths were followed by single-wavelength stopped-flow using a monochromator, and the whole spectral changes were monitored by rapid-scan stopped-flow using a diode-array accessory. Global analysis of the rapid-scan data was conducted using the Pro-Kineticist (Applied PhotoPhysics). The association rate constants of CO and NO, $k_{on}$(CO), and $k_{on}$(NO), respectively, were measured by different methods.

In the case of CO binding, the observed rates, $k_{obs}$, of single-wavelength data under pseudo-first-order conditions, were obtained by fitting time courses of absorbance to the standard exponential function:

$$A = A_f + ae^{-k_{obs} \times t}, \quad (1)$$

where $A_f$, $t$, and $a$ are the final optical absorbance, reaction time, and amplitude of the total optical change, respectively. The second-order association rate constant in CO binding, $k_{on}$(CO), was derived from the slopes in the secondary plots of $k_{obs}$ versus [CO]:

$$k_{obs} = k_{on} \times [CO] + k_{off}, \quad (2)$$

where the $y$-intercept corresponds to $k_{off}$(CO).

The much faster formation rate of a six-coordinate (6c) NO–heme–His complex in DHP, $k_{on}$(NO), was measured under the conditions of true second-order reaction [31], by rapidly mixing ferrous DHP with stoichiometric NO, and obtaining the $k_{obs}$ by fitting the time course to the following equation:

$$A = A_f + \frac{\Delta A_0}{(\Delta A_0 \times k_{obs} \times t + 1)}, \quad (3)$$

where $A_f$ is the final optical absorbance and $\Delta A_0 = A_i - A_f$ ($A_i$ is the initial absorbance); $t$ is the reaction time. Second-order rate constant, $k_{on}$(NO) in unit of $M^{-1}$ $s^{-1}$, was obtained by multiplying $k_{obs}$ with the difference extinction coefficient, $\Delta\varepsilon$, between the reactant DHP and the product, 6c NO–heme–His complex. [NO] did not decay noticeably during the experiments due to the well-maintained anaerobic conditions, as demonstrated by the high reproducibility of the multiple stopped-flow reactions. Moreover, there is little concern for residual oxygen in the anaerobic chamber due to the slow third-order reaction between NO and $O_2$ [32]. Any residual $Na_2S_2O_4$ left in the anaerobic DHP sample did not affect the kinetic measurement of the NO binding to DHP either, since NO binds to DHP at a rate faster by several orders of magnitude than it reacts with $Na_2S_2O_4$.

The $k_{off}$(CO) constants in DHP were very small, and the accurate values based on the $y$-intercepts of secondary plots were inaccurate due to large potential errors obtained by fitting. The $k_{off}$(CO) constants were determined using an NO competition method by reacting the 6c CO complex with 1 mM NO. On the other hand, the $k_{off}$(NO) constants were determined by sequential mixing stopped-flow spectrophotometry. DHP was reacted with 1× NO in the first mixing to form the 6c NO complex; the reaction mixture was allowed to age for 100 ms, and then reacted with 500 μM CO to replace NO, in the presence of 12.5 mM $Na_2S_2O_4$ to consume dissociated NO to minimize its reassociation.

## EPR spectroscopy

EPR spectra were recorded on a Bruker EMX spectrometer (Billerica, MA) at 115 K. Data analyses and spectral simulations were conducted using WinEPR and SimFonia programs furnished with the EMX system. EPR was conducted using the following parameters: frequency, 9.28 GHz; power, 4 mW; modulation frequency, 100 kHz; modulation amplitude, 2.5 G, and time constant, 0.33 s.

EPR samples of 6c NO complex were prepared by injecting desired volumes of 2 mM NO stock into and mixing with anaerobic ferrous DHP inside EPR tubes. The reactions were conducted inside the anaerobic chamber, and the EPR samples were then transferred outside the chamber, quickly frozen in a dry ice/ethanol mixture. The time between the NO injection and sample freezing was less than 1 min.

## Computer fitting

Multiple time courses of $A_{431}$ during the ferrous DHP reactions with different [$O_2$] under pseudo-first-order conditions were fit simultaneously using the SCoP Program (Simulation Resources, Inc., Redlands, CA), based

Biochemical Journal (2017) **474** 3485–3498
DOI: 10.1042/BCJ20170515

**Table 2 Association and dissociation rate constants of gaseous ligand binding to ferrous DHP**

| | $k_{on}$ ($M^{-1}$ $s^{-1}$) | | $k_{off}$ ($s^{-1}$) | |
|---|---|---|---|---|
| | NO | CO | NO | CO |
| DHP A | $1.1 \times 10^8$ | $1.5 \times 10^6$ | $3.6 \times 10^{-3}$ | 1.0 |
| H55D DHP A | $1.5 \times 10^8$ | $2.7 \times 10^6$ | $4.6 \times 10^{-3}$ | 0.9 |
| H55V DHP A | $2.7 \times 10^8$ | $2.4 \times 10^6$ | $4.0 \times 10^{-3}$ | 0.5 |
| DHP B | $1.7 \times 10^8$ | $0.8 \times 10^6$ | $4.0 \times 10^{-3}$ | 0.7 |

on the global minimization following the principal axis method (PRAXIS) [33]. The model used was based on the one-step reaction:

$$\text{deoxyferrous DHP} + O_2 \leftrightarrow \text{oxyferrous DHP}.$$

The parameters allowed to float in the fittings were the forward/reverse rate constants, and the preset floating ranges were 10–1000 $\mu M^{-1}$ $s^{-1}$ and 1–100 000 $s^{-1}$ for the forward and reverse rate constants, respectively.

# Results

## CO binding to ferrous DHP

The rapid-scan stopped-flow reaction of ferrous DHP A with CO exhibited a spectral change consistent with two-state (single-step) kinetics. The Soret peak shifted from 429 to 422 nm with no spectral intermediate (Figure 1A), indicating the formation of a six-coordinated low-spin (6cLS) CO–heme–His complex at 422 nm starting from a deoxy five-coordinated high-spin (5cHS) heme at 429 nm. The spectrum of the 6c CO–heme–His complex was resolved from the data based on a simple $A \rightarrow B$ model (Figure 1A, inset). Observed rates, $k_{obs}$s, obtained by fitting the time courses of $A_{422}$ at various [CO], exhibited a linear dependence on [CO] (Figure 1B). The second-order association rate constant, $k_{on}$(CO) as the slope, was $1.5 \times 10^6$ $M^{-1}$ $s^{-1}$ (Figure 1B and Table 2). The $k_{on}$(CO) constants of DHP B, H55D, and H55V DHP A measured by the same method were $0.8 \times 10^6$, $2.7 \times 10^6$, and $2.4 \times 10^6$ $M^{-1}$ $s^{-1}$, respectively (Table 2). On the other hand, the dissociation rate constant of the CO complex in DHP A, $k_{off}$ (CO), was measured with the NO competition method following the time course of $A_{422}$ (Figure 1C). The $k_{off}$(CO) of DHP A was determined as 1.0 $s^{-1}$ (Table 2). Similarly measured, the $k_{off}$(CO)s of DHP B, H55D, and H55V DHP A were 0.7, 0.9, and 0.5 $s^{-1}$, respectively (Table 2). The binding constants, calculated as $K_D(CO) = k_{off}(CO)/k_{on}(CO)$, were $6.7 \times 10^{-7}$, $3.4 \times 10^{-7}$, $2.1 \times 10^{-7}$, and $8.3 \times 10^{-7}$ M for wt, H55D and H55V DHP A, and DHP B, respectively (Table 3).

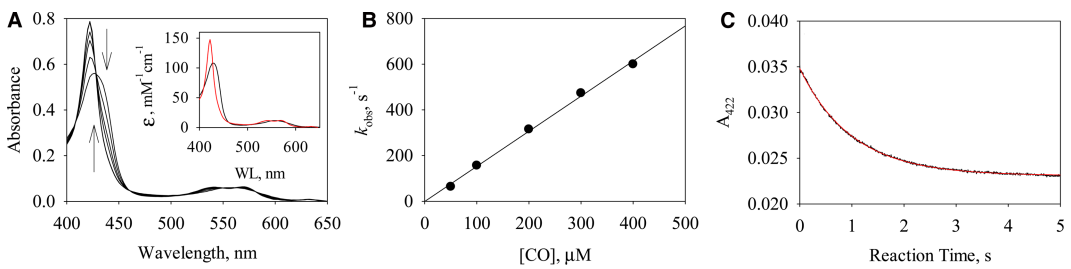


**Figure 1. Kinetics of CO binding to DHP A.**

(**A**) During the rapid-scan reaction of 5 μM DHP A with 50 μM CO, the spectra at 1.28, 6.4, 14.1, 24.3, 49.9, 75.5, and 101.1 ms are presented. Arrows represent the directions of the spectral changes. (inset) Deconvoluted optical species from the rapid-scan data based on a single-step reaction model $A \rightarrow B$: *A* (black), ferrous DHP A; *B* (red), CO–heme–His complex. (**B**) The linear fit (line) of $k_{obs}$ of 5 μM ferrous DHP A reactions with CO to [CO] (circle). The $k_{obs}$s were from fitting the time courses of $A_{422}$ to eqn (1). (**C**) Time course of $A_{422}$ during the reaction of 0.25 μM DHP A CO complex with 1 mM NO (black line) is shown. The red line represents the fit to eqn (1).

Biochemical Journal (2017) **474** 3485–3498
DOI: 10.1042/BCJ20170515

**Table 3 Dissociation constants of gaseous ligands to ferrous DHP**

| | $K_D$(NO), M | $K_D$(CO), M | $K_D$($O_2$), M |
|---|---|---|---|
| DHP A | $3.3 \times 10^{-11}$ | $6.7 \times 10^{-7}$ | $1.1 \times 10^{-5}$ |
| H55D DHP A | $3.1 \times 10^{-11}$ | $3.4 \times 10^{-7}$ | $1.2 \times 10^{-4}$ |
| H55V DHP A | $1.5 \times 10^{-11}$ | $2.1 \times 10^{-7}$ | $4.6 \times 10^{-4}$ |
| DHP B | $2.4 \times 10^{-11}$ | $8.3 \times 10^{-7}$ | $1.8 \times 10^{-5}$ |

## NO binding to ferrous DHP

When ferrous DHP A was reacted with stoichiometric NO, the Soret peak quickly shifted from 429 to 420 nm, indicating the formation of a 6c NO–heme–His complex (Figure 2A). The optical spectrum of the 6c NO–heme–His complex was resolved from the rapid-scan data based on model $A \rightarrow B$ (Figure 2A, inset). The EPR spectrum of the DHP A reacting with stoichiometric NO exhibited features which were readily simulated using nitrogen hyperfine splitting constants, typical of a 6c NO complex (Figure 3A,B), in line with the observation based on the optical data. However, it was difficult to obtain accurate $k_{obs}$ for NO complex formation under pseudo-first-order conditions due to the much faster formation rate of NO complex compared with that of CO complex. The formation rate constant of the 6c NO complex, $k_{on}$(NO), was determined with a single-wavelength stopped-flow measurement at 430 nm under true second-order reaction conditions, reacting 0.7 μM DHP A with stoichiometric NO. About 90% of the time course was captured, enabling a good fit to eqn (3), $k_{on}(NO) = 1.1 \times 10^8\ M^{-1}\ s^{-1}$ (Figure 2B and Table 2). The $k_{on}$(NO)s of DHP B, H55D, and H55V DHP A measured with the same method were $1.7 \times 10^8$, $1.5 \times 10^8$, and $2.7 \times 10^8\ M^{-1}\ s^{-1}$, respectively (Table 2). On the other hand, the dissociation rate constant of the 6c NO–heme–His complex, $k_{off}$(NO), was obtained by the CO competition method in the presence of excess $Na_2S_2O_4$ and fitting the time course of $A_{422}$ to eqn (1) (Figure 2C). The rate was much slower than $k_{on}$(CO) of DHP A (Table 2), confirming that formation of the CO complex under these experimental conditions was rate-limited by $k_{off}$(NO), $3.6 \times 10^{-3}\ s^{-1}$. The $k_{off}$(NO) was measured in the same way for H55D, H55V DHP A, and DHP B, $4.6 \times 10^{-3}$, $4.0 \times 10^{-3}$, and $4.0 \times 10^{-3}\ s^{-1}$, respectively (Table 2). The $K_D$(NO)s calculated as $k_{off}$(NO)/$k_{on}$(NO) were $3.3 \times 10^{-11}$, $3.1 \times 10^{-11}$, $1.5 \times 10^{-11}$, and $2.4 \times 10^{-11}$ M, for wt, H55D and H55V DHP A, and DHP B, respectively (Table 3).

The heme–His bond was stable in the 6c NO–heme–His complex formed in the reaction of DHP A with stoichiometric NO, as indicated by the lack of further optical change after its formation (data not shown). The stability of the 6c NO–heme–His complex is corroborated by the EPR spectrum of the DHP A reaction with stoichiometric NO, which exhibits features typical of the 6c NO complex (Figure 3A). EPR data also demonstrated that DHP A does not exhibit multiple-step NO binding, which is distinct from the behavior of gas heme

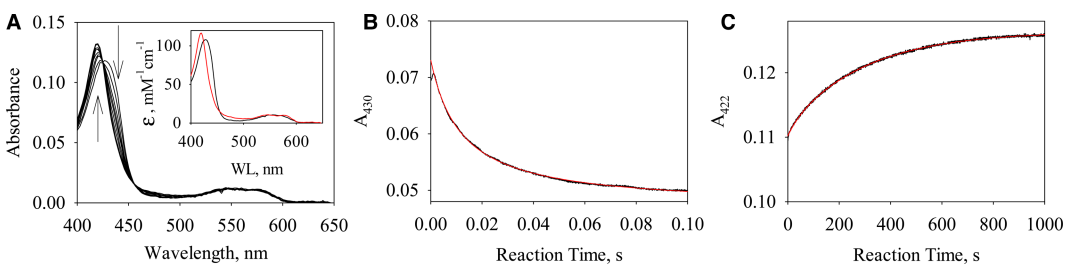


**Figure 2. Kinetics of NO binding to DHP A.**

(**A**) The spectra captured at 1.28, 3.84, 6.4, 8.96, 11.5, 16.6, 24.3, 37.1, and 49.9 ms during the rapid-scan reaction of 1.1 μM DHP A with 1× NO are shown. Arrows represent the directions of the spectral changes. (inset) Deconvoluted optical species from the rapid-scan data based on a single-step reaction model $A \rightarrow B$: *A* (black), ferrous DHP A; *B* (red), 6c NO–heme–His complex. (**B**) Time course of $A_{430}$ during the reaction of 0.7 μM ferrous DHP A with 1× NO (black line). The association rate constant of DHP A 6c NO–heme–His complex, $k_{on}$(NO), was obtained by fitting to eqn (3) (red line). (**C**) Time course of $A_{422}$ in the dissociation of the 6c NO–heme–His complex in DHP A (black). DHP A was first reacted with 1× NO; after 100 ms, the reaction mixture was further reacted with 500 μM CO plus 12.5 mM $Na_2S_2O_4$ (black line). Red line: fit to eqn (1).

Biochemical Journal (2017) **474** 3485–3498
DOI: 10.1042/BCJ20170515

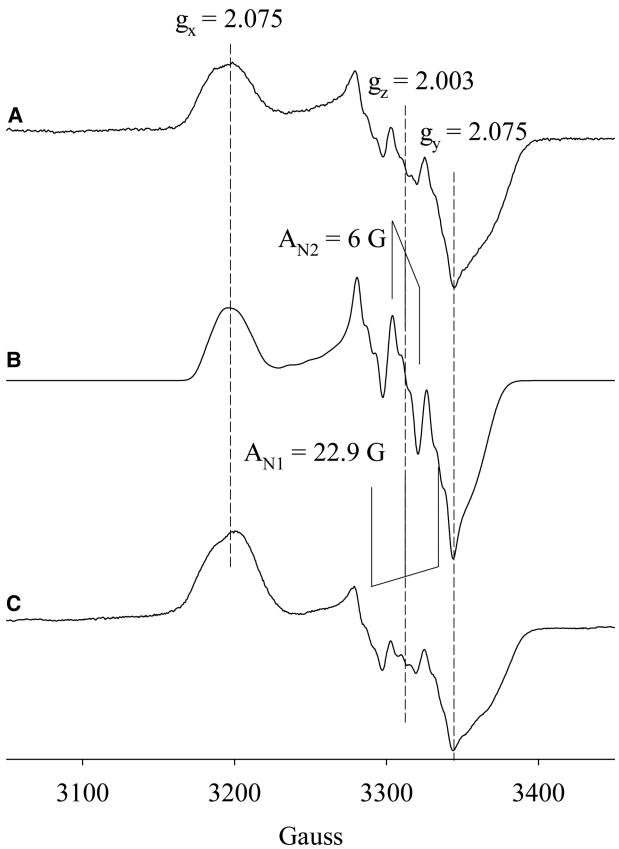


**Figure 3. EPR spectra of DHP A 6c NO–heme–His complexes.**

(**A**) EPR spectrum of the NO complex formed by reacting DHP A with 1× NO. (**B**) Simulation of A using the following parameters: $g_x = 2.075$, $g_y = 1.984$, $g_z = 2.003$; $A_{N1}$: $A_x = 10$ G; $A_y = 15$ G and $A_z = 22.9$ G; $A_{N2}$: $A_x = A_y = A_z = 6$ G. (**C**) EPR spectrum of the NO complex formed by reacting DHP A with 11× NO.

sensors such as sGC [34]. In the reaction of DHP A with up to 11 equivalents of NO, the 6c NO–heme–His remained stable as shown by the identical EPR spectra under these conditions (Figure 3A,C). The anisotropic EPR spectrum exhibited a nine-line hyperfine splitting of the center $g_z$ component (2.003), which was best simulated by a three-line hyperfine splitting ($A = 22.9$ G) from the NO nitrogen and three-line super hyperfine ($A =$ 6 G) from the proximal histidine ε-nitrogen (Figure 3B). The hyperfine features for the $g_x$ (2.075) and the $g_y$ (1.984) components were not easily observed due to smaller hyperfine splittings and broader linewidth [35].

## Reaction of $O_2$ with ferrous DHP

The rapid-scan stopped-flow reaction of ferrous DHP A with 30 μM $O_2$ proceeded rapidly and finished within 4 ms (Figure 4A). No optical intermediate was observed. However, the α/β bands were poorly resolved at 556 and 549 nm, indicating that the oxyferrous complex did not fully develop at [$O_2$] of 30 μM. When ferrous DHP A was reacted with 100 μM $O_2$, the first spectrum captured was that typical of an oxyferrous complex with better resolved α and β bands at 541 and 577 nm, respectively (Figure 4B), indicating more complete formation of the oxyferrous complex (Figure 4B). The rapid-scan data, therefore, indicated a sizeable $k_{off}(O_2)$ for the oxyferrous complex. In single-wavelength stopped-flow measurements, when DHP A was reacted under pseudo-first-order conditions with $O_2$ of various concentrations, all the $k_{obs}$s except for that with the lowest concentration of $O_2$ were ≥500 $s^{-1}$, which was sufficiently large and that majority of the reactions occurred in the dead time of the stopped-flow apparatus (Figure 4C), corroborating the large $k_{obs} = k_{on}[O_2] + k_{off}$ of DHP A. Therefore, only very small factions of reactions were captured (Figure 4C), and $k_{obs}$s could not be measured to construct a secondary plot of $k_{obs}$ versus [$O_2$], in contrast with the case of $k_{on}$(CO) measurement (Figure 1B). Moreover, the $k_{on}(O_2)$ to DHP A cannot be measured under true second-order reaction conditions

Biochemical Journal (2017) **474** 3485–3498
DOI: 10.1042/BCJ20170515

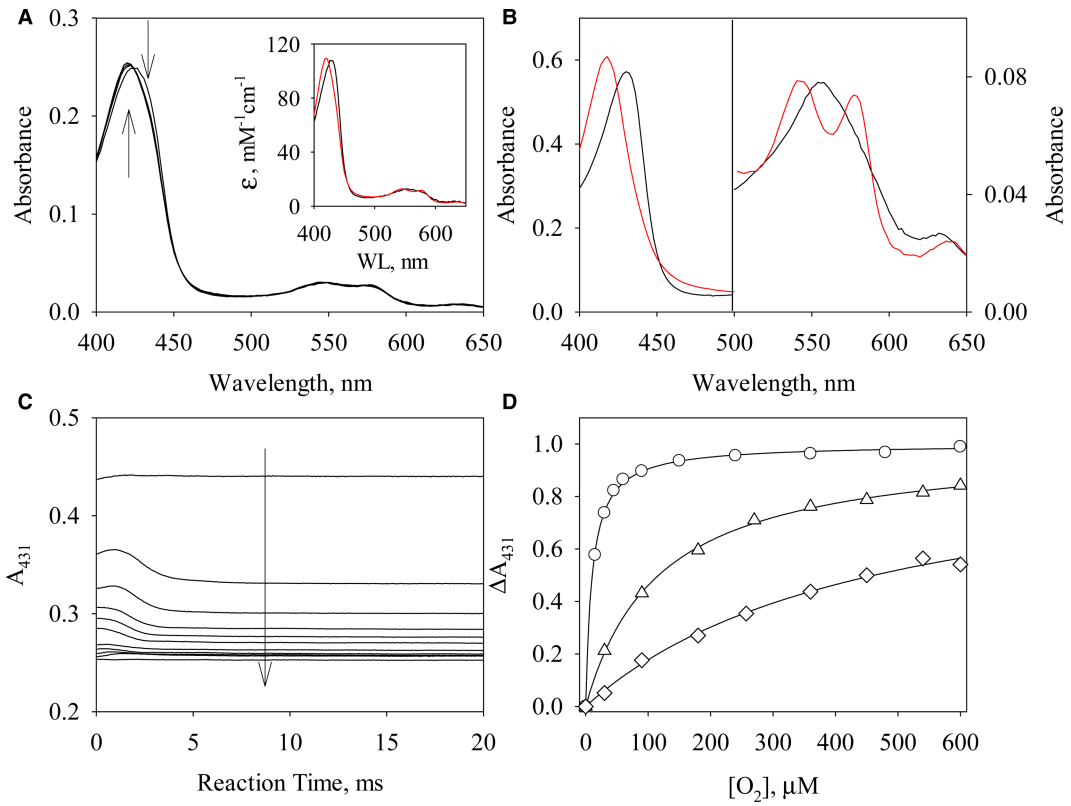


**Figure 4. Kinetics of $O_2$ binding to DHP A.**

(**A**) The spectra captured at 1.28, 3.84, 6.4, 8.96, and 11.5 ms during the rapid-scan reaction of 2.4 μM DHP A with 30 μM $O_2$. Arrows represent the directions of the spectral changes. (inset) Deconvoluted optical species from the rapid-scan data based on a single-step reaction model $A \rightarrow B$: *A* (black), ferrous DHP A; *B* (red), oxyferrous complex. (**B**) The spectrum captured at 1.28 ms during the reaction of 5.3 μM DHP A with 100 μM $O_2$ (red), in comparison with the spectrum of ferrous DHP A (black). (**C**) Time courses of $A_{431}$ in the 4.1 μM ferrous DHP A reactions with various concentrations of $O_2$. The arrow indicates the increase in [$O_2$]: 0 (anaerobic buffer, top), 15, 30, 45, 60, 90, 150, 240, 360, 480, and 600 μM. (**D**) Normalized $\Delta A_{431}$ versus [$O_2$]. $\Delta A_{431} = A_{431,\mathrm{DHPA+buffer}} - A_{431,\mathrm{DHPA+O_2}}$ and each $A_{431}$ was averaged over 10 – 20 ms. To compare the $\Delta A_{431}$ in different proteins, $\Delta A_{431}$ was normalized against the $A_{431,\mathrm{max}}$ obtained by fitting to eqn (4). Circle: wt DHP A; triangle: H55D DHP A; diamond: H55V DHP A, and lines: the fits.

by reacting DHP A with stoichiometric $O_2$, like that for NO binding (Figure 2B). The method of fitting to a second-order reaction eqn (3) fails due to the very large $k_{\mathrm{off}}(O_2)$, which could not be determined using the CO or NO competition method. Actually, the $\Delta A_{422}$ observed in the reaction of the oxyferrous DHP A with 500 μM CO plus 12.5 mM $Na_2S_2O_4$ only accounted for ~5% of the total $\Delta A_{422}$ by CO complex formation and the reactions were rate-limited by $k_{\mathrm{on}}(CO)$ (data not shown).

Although no kinetic parameters were measured, the affinity of DHP A for $O_2$ was experimentally determined due to that the decrease in DHP A Soret signal was dependent on [$O_2$], and all the reactions reached equilibrium after 10 ms (Figure 4C). It was therefore possible to measure $K_D(O_2)$ of ferrous DHP A by titrating it with $O_2$ and monitoring the [$O_2$]-dependent Soret absorbance change at equilibrium using single-wavelength stopped-flow measurements. The plot of the observed absorbance change versus [$O_2$] was successfully fit with the following equation:

$$\Delta A_{431} = \frac{\Delta A_{431,\mathrm{max}} \times [O_2]}{(K_D(O_2) + [O_2])}. \quad (4)$$

The $K_D(O_2)$ of DHP A thus obtained was 11 μM (Figure 4D and Table 3).

Biochemical Journal (2017) **474** 3485–3498
DOI: 10.1042/BCJ20170515

The time courses of $A_{431}$ in the reactions of DHP B with various levels of $O_2$ were quite similar to those of DHP A (Supplementary Figure S1B), and the $K_D(O_2)$ of DHP B, 18 μM (Table 3), was determined using the same $O_2$-titration method. Almost no kinetic change was captured during the reactions of H55D and H55V DHP A even with lowest concentration of $O_2$ (Supplementary Figure S1C,D), likely due to larger $k_{off}(O_2)$s. Nevertheless, $K_D(O_2)$s of H55D and H55V DHP A were determined using the $O_2$-titration method. Mutation of His55 to polar aspartate apparently led to a significantly lower affinity of H55D DHP A for $O_2$, $K_D(O_2)$ = 120 μM (Supplementary Figure S1C and Table 3). The affinity for $O_2$ was even lower for DHP A with His55 conversion to apolar valine, $K_D(O_2)$ = 460 μM (Supplementary Figure S1D and Table 3).

# Discussion

The CO rebinding kinetics of DHP triggered by flash photolysis have been studied as a function of temperature using the FTIR temperature derivative spectroscopy [36]. To build further on the low temperature data, the full set of CO and NO association/dissociation kinetics of DHP at ambient temperature has been measured in the present study. The kinetic studies are supported by many structural studies of DHP. The crystallographic data of CO complex of ferrous DHP and varieties of spectroscopic characterizations revealed two conformations of His55, 'open' and 'closed' [11,16,37]. Unlike the relative strong hydrogen bonding between CO and distal residue(s) that is observed in truncated Hbs from *Bacillus subtilis* [38] and truncated-II Hb from *Mycobacterium tuberculosis* [39], the hydrogen bonding interaction between axially bound CO and distal His55 in DHP is relatively weak. Nevertheless, previous structural, spectroscopic, and QM/MM studies all suggest that the structural perturbation in these Hbs is a result of enhanced flexibility of distal residue sidechain in the distal pocket [37]. Although the hydrogen bonding scheme changes from the 'closed' to the 'open' conformation of distal His55 in the CO complex, only a single set of $k_{on}$(CO) and $k_{off}$(CO) values was obtained in our binding kinetic measurements, indicating that the dynamic His55 conformational switch is in fast equilibrium and has a minimal effect on the CO-binding kinetics at ambient temperature. The minimal effect of the 'closed' ↔ 'open' conformational switch on CO binding is corroborated by the molecular dynamics (MD) calculation on the His55 mutants [37]. Although MD is limited to 20 ns, too short for the trajectory of any gaseous ligand in its binding to DHP, it indicates that residue 55 is locked in a single conformation in the two His55 DHP A mutants, 'closed' in H55V and 'open' in H55D mutants, respectively [37]. Nonetheless, the kinetics of CO binding in these two mutants remains unchanged compared with that of wt DHP A (Table 2).

In the crystallographic structure of DHP A CO complex (PDB 4GZG), the distal histidine of 6cLS DHP CO complex is primarily in the solvent exposed conformation, due to the interaction between His55 and the two propionate groups on the heme [37]. Resonance Raman data for the CO complex or DHP also showed one, not two, vibrational frequencies for Fe(II)–CO [40]. FTIR data also show one dominant C–O stretching at room temperature [36]. Similar to the cases of SWMb and model compound Fe(II)PP(1-MeIm) [41,42], the binding of both CO and NO to DHP A and B is a single-step process that leads to a stable 6c complex. The stable 6c NO complex in DHP is in contrast with those in sGC and some bacterial heme nitric oxide and oxygen-binding proteins (H-NOXs), which are unstable and subsequently convert into stable 5c NO–heme complexes [28,43–46].

The binding parameters, $k_{on}/k_{off}/K_D$ of DHP (Tables 2 and 3), are very different from those of Mb and a model heme [28,29]. Despite their common globin protein folds and similar heme pockets (Supplementary Figure S2), the $k_{off}$ and $k_{on}$ constants of DHP are ∼2–3 orders larger and ∼1 order smaller than those of SWMb, respectively. These differences lead to $K_D$s of DHP that are ∼3 orders of magnitude larger than those of SWMb. On the other hand, the binding parameters of the first-binding step to form 6c complexes are quite similar to those of the bacterial H-NOXs [28,43–46], even though they have totally different structural folds. Bioinformatic graphical analysis of the $K_D$ from many hemeproteins concludes that the main factors that caused the 8–9 order range spread in $K_D$ values are heme distal steric hindrance and the proximal constraint [28,29]. Thus, such similarities in binding parameters suggest that the proximal strains and distal steric hindrance around heme are similar in DHP and H-NOXs. This point will be further discussed below.

The values of $K_D(O_2)$ of DHP are 11 and 18 μM for DHP A and B, respectively (Table 3), and are reasonably close to the published values 7.7 and 4 μM, respectively, measured with a different method [24]. The differences can arise from the stopped-flow titration method used in the present study and the previous competition method between $O_2$ ligand and *t*-butyl isocyanide. The relatively larger difference in $K_D(O_2)$ of DHP B from the two studies is not clear at this time. The different $K_D(O_2)$ between DHP A and B may be due

Biochemical Journal (2017) 474 3485–3498
DOI: 10.1042/BCJ20170515

to steric differences in the distal pockets, probably caused by the subtle effects of the amino acid differences between the two isozymes.

Single-wavelength stopped-flow data revealed that $O_2$-binding to DHP has a large dissociation rate, $k_{on}[O_2] + k_{off} \geq 500\ s^{-1}$, in sharp contrast with that of SWMb, $k_{off} \sim 15\ s^{-1}$ Though not determined experimentally, the $k_{on}(O_2)$ and $k_{off}(O_2)$ constants of DHP were estimated by multiple nonlinear regression analysis of kinetic data acquired at various $[O_2]$ (Supplementary Figure S1). The association rate constants, $k_{on}(O_2)$, obtained from nonlinear regression were similar for both DHP isozymes and His55 mutants, $3.0 \times 10^7$, $2.0 \times 10^7$, $1.9 \times 10^7$, and $9.9 \times 10^6\ M^{-1}\ s^{-1}$, for wt DHP A and B, H55D, and H55V DHP A, respectively (Supplementary Table S1). On the other hand, $k_{off}(O_2)$s of His55 mutants are noticeably larger than those of wt DHP A and B, $4.1 \times 10^3$ and $2.1 \times 10^3\ s^{-1}$ for H55V and H55D DHP A, respectively, and $2.7 \times 10^2$ and $2.9 \times 10^2\ s^{-1}$ for wt DHP A and B, respectively (Supplementary Table S1).

The $k_{on}(O_2)$ and $k_{off}(O_2)$ constants of DHP estimated by the computer fitting corroborates the H-bonding strength between $O_2$ and $^{\varepsilon}N$ of His55 in the distal heme pocket, implicated by the $^{\varepsilon}N$–Fe distance in DHP, which is intermediate between those of Mb and HRP. The $O_2$ ligand is oriented in a 'side on' conformation in Mb to form a stable Fe(II)–$O_2$ complex for oxygen storage or transfer and an 'end on' conformation in HRP to facilitate the heterolytic cleavage of O–O bond in its peroxidase catalysis [47]. The intermediate $^{\varepsilon}N$–Fe distance and the very flexible His55 switching dynamics in DHP not only provide it the versatility as a multifunctional hemeprotein, but also lead to a less stable Fe(II)–$O_2$ intermediate than that of Mb. The capability in forming a Fe(II)–$O_2$ intermediate affords DHP activities, including mono-oxygenase, oxidase, and dioxygenase; and its interaction with $H_2O_2$ enables it both peroxidase and peroxygenase activities.

Based on the rate constants and binding constants obtained for all three gaseous ligands, we are in a position to assess whether DHP follows the 'sliding scale rule'. The rule based on the bioinformatic graphical analyses conducted for more than 100 hemeproteins and model compound provides trends that are conserved within various functional classes of hemeproteins [28,29].

The bioinformatic analysis provides five important conclusions regarding NO, CO, and $O_2$ bindings to hemeproteins [28]. (1) The large $K_D(CO)/K_D(NO)$ and $K_D(O_2)/K_D(CO)$ ratios, $10^3$–$10^4$, apply to 5c hemeproteins that have a neutral proximal histidine ligand, whereas much smaller differences in ligand affinities occur in other hemeproteins with proximal ligands of imidazolate, cysteine thiolate, or tyrosine phenolate anion. (2) Distal steric hindrance (typified by cytochrome $c'$) and proximal strain (illustrated by sGC) are the two dominating factors that can lead to dramatic $10^8$–$10^9$-fold changes in $K_D$ for all three gaseous ligands, but remarkably cause little change in the $K_D(CO)/K_D(NO)$ and $K_D(O_2)/K_D(CO)$ ratios. These nearly constant ratios determine that log $K_D$(NO)–log $K_D$(CO)–log $K_D(O_2)$ lines of different heme sensors remain parallel to each other in the 'sliding scale rule' plot. (3) As a result, for a heme sensor, determination of the $K_D$ for one ligand (i.e. CO) allows estimation of the $K_D$ values for the other two ligands, which is particularly useful for hemeproteins with very high ($>10^{-3}$ M) $K_D$ values for $O_2$ binding. (4) Although $K_D$(CO) in a hemeprotein is determined by the distal steric hindrance and proximal strain, some hemeproteins have other structural elements which specifically enhance their affinities for $O_2$ and/or NO. The presence of an H-bond donor(s) on the distal side of heme preferentially enhances(enhance) $O_2$ affinity, but have little or no effect on CO or NO binding, leading to deviation from the 'sliding scale rule' at the log $K_D(O_2)$ end. (5) The ultra-high apparent affinities of some heme sensors for NO, such as sGC and certain bacterial H-NOXs, are due to multiple-step NO binding in which the unstable 6c NO–heme–His complex either promptly converts to a 5c NO–heme complex or react rapidly with secondary NO to generate a 5c NO–heme complex. The $K_D$s of the initial 6c Fe(II)–NO complexes in these heme sensors follow the 'sliding scale rule'; however, the subsequently generated 5c NO complexes have significantly smaller $k_{off}$ constants, leading to much lower apparent $K_D$s [28,29].

The graphical analysis shown in Figures 5 and 6 not only reveals the gaseous ligand selectivity of DHP, but also its binding behavior relative to other hemeproteins, some of them with very different functions and protein folds. The log $K_D$s of wt, H55D and H55V DHP A, and wt DHP B are plotted versus ligand type, together with either those of various globins (Figure 5) or nonglobins (Figure 6). The nonglobins include H-NOXs from *Nostoc* sp. (*Ns* H-NOX) and *Thermoanaerobacter tengcongensis* (*Tt* H-NOX), cytochrome $c'$, and model heme (Figure 6). The lines connecting log $K_D$(NO) and log $K_D$(CO) for each hemeprotein are parallel aside from slight deviations due to the random variations during the measurements or slight differences in the experimental conditions.

For H64V SWMb and *Ns* H-NOX, which do not have a H-bond donor to stabilize Fe(II)–$O_2$, their log $K_D$(NO), log $K_D$(CO), and log $K_D(O_2)$ almost fall on straight lines (Figures 5A and 6A). On the other hand,

Biochemical Journal (2017) **474** 3485–3498
DOI: 10.1042/BCJ20170515

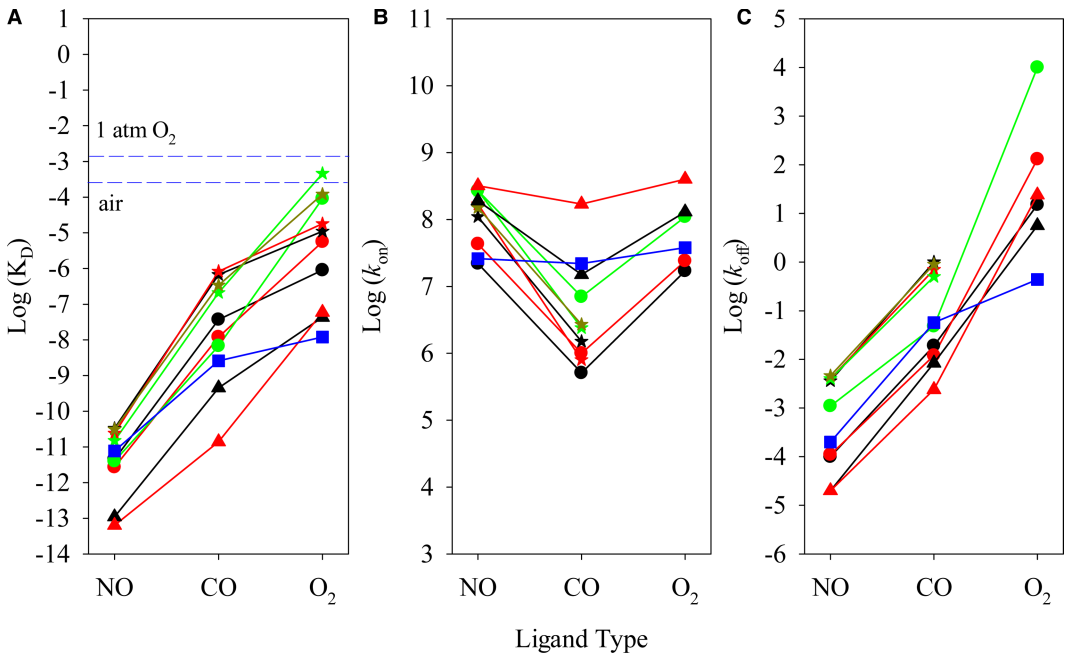


**Figure 5. Relationship of log $K_D$, log $k_{on}$, and log $k_{off}$ of NO, CO, and $O_2$ for DHP and other globins versus ligand type.**
The measured values of $K_D$ (**A**), $k_{on}$ (**B**), and $k_{off}$ (**C**) for NO/CO/$O_2$ of ferrous DHP are plotted on a logarithmic scale versus ligand type. Parameters measured for different globins, including SWMb and mutants, soybean leghemoglobin (Lb) and its H61L mutant, and flavohemoglobin (FHb), are plotted for comparisons. The values of the parameters are from [28] and the references therein. DHP A, black star; DHP B, red star; H55D DHP A, dark yellow star; H55V DHP A, green star; SWMb, black circle; H64Q Mb, red circle; H64V Mb, green circle; Lb, black triangle; H61L Lb, red triangle; FHb, blue square.

Fe(II)–$O_2$ complexes in SWMb and *Tt* H-NOX are stabilized by distal His64 or Tyr140, respectively, leading to downward sloped log $K_D$(CO)–log $K_D$($O_2$) lines relative to their upward log $K_D$(NO)–log $K_D$(CO) lines (Figures 5A and 6A). In wt DHP A and B, Fe(II)–$O_2$ is also stabilized by H-bonding to distal His55, resulting in lower log $K_D$($O_2$)s which deviates from the extrapolation of the corresponding log $K_D$(NO)–log $K_D$(CO) lines (Figure 5A). In H55D DHP A, the Fe(II)–$O_2$ is less stabilized compared with wt DHP A due to the loss of distal His55, reflected by the ~8-fold increase in $k_{off}$($O_2$) of H55D DHP A compared with that of wt DHP A (Supplementary Table S1). Nonetheless, a hydrogen bonding network through $H_2O$ may still provide some stabilization for the Fe(II)–$O_2$ complex [48], lowering $K_D$($O_2$) for H55D DHP A from the extrapolation of its log $K_D$(NO)–log $K_D$(CO) line to 117 μM. In H55V DHP A, $K_D$($O_2$) further increases to 460 μM, presumably due to the substitution of His55 with a nonpolar valine residue, which is not capable of supporting hydrogen bonding through its sidechain, as indicated by another 2-fold increase in $k_{off}$($O_2$) in H55V DHP A compared with that of the H55D mutant (Supplementary Table S1).

Thus, from H55V, H55D, to wt DHP A, a progressively increasing effect of the H-bond donor strength in stabilizing the Fe(II)–$O_2$ complex is clearly illustrated. A similar systematic effect on $O_2$ affinity can be observed by manipulating the H-bonding strength in wt, H64Q, and H64V Mb where $K_D$($O_2$) increases from 0.88 to 5.6 to 91 μM (Figure 5A) [49–51]. The effects of H-bonding donor observed for both DHP and Mb are only selective for $O_2$ binding and show essentially no effect on CO or NO binding. Overall, the gaseous ligand selectivity of DHP agrees well with the 'sliding scale rule' hypothesis. By removing the H-bonding donor, as observed in the H55V mutant, DHP exhibits good selectivity between NO/CO and CO/$O_2$ pairs, each with 3–4 orders separation in binding affinities (Table 3 and Figure 6).

The selective binding of DHP to the gaseous ligands presents a sharp contrast with those of typical peroxidases such as HRP and CCP, which show very poor gaseous ligand selectivity due to the presence of a strong electron-donating imidazolate proximal ligand. DHP is structurally more similar to globins, such as Mb and Hb (Supplementary Figure S2), than peroxidases despite its peroxidase activity. The presence of a neutral proximal imidazole ligand in DHP confers a high degree of selectivity among NO, CO, and $O_2$. Based on this

Biochemical Journal (2017) **474** 3485–3498
DOI: 10.1042/BCJ20170515

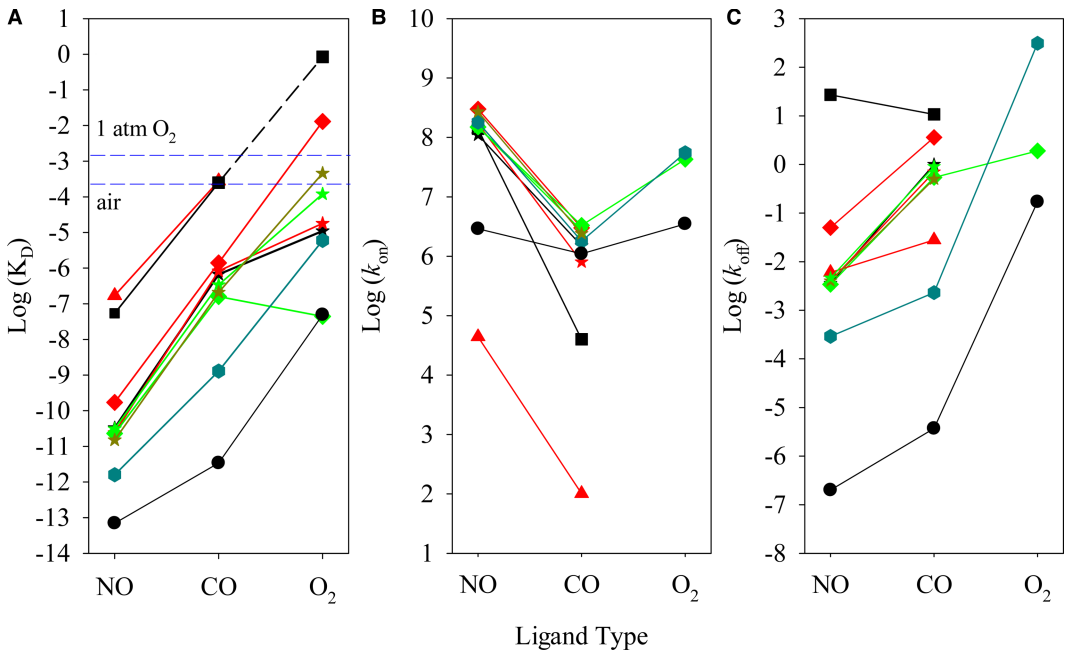


**Figure 6. Relationship of log $K_D$, log $k_{on}$, and log $k_{off}$ of NO, CO, and $O_2$ for DHP and nonglobin hemeproteins versus ligand type.**

The measured values of $K_D$ (**A**), $k_{on}$ (**B**), and $k_{off}$ (**C**) for NO/CO/$O_2$ on ferrous DHP are plotted on a logarithmic scale versus ligand type, in comparisons with those of wt and L16A cyt *c*′, *Ns* and *Tt* H-NOXs, and heme model Fe(II)PP(1-MeIm) to show the large dynamic range of $K_D$, $k_{on}$, and $k_{off}$ values modulated by the different heme-binding environments. DHP A, black star; DHP B, red star; H55D DHP A, green star; H55V DHP A, dark yellow star; human sGC, black square; *Ns* H-NOX, red diamond; *Tt* H-NOX, green diamond; Fe(II) PP(1-MeIm), cyan hexagon; cyt *c*′, red triangle; L16A cyt *c*′, black circle.

rationale, other enzymes that show peroxidase activity and possess a neutral histidine proximal ligand should also show good discrimination among the three gaseous ligands. Prostaglandin H synthase (also known as a cyclooxygenase) [52] will provide a good test of this hypothesis since it has a neutral proximal histidine heme ligand and is a much more efficient peroxidase than DHP.

# Conclusions

We have measured the binding of three gaseous ligands, CO, NO, and $O_2$, to DHP and two of its mutants to further test the 'sliding scale rule' hypothesis. Recent work to assess six different H-NOXs including sGC with the same type of protein scaffold in order to gain insights into the functional differences among them has revealed significant differences especially in the multiple-step NO binding, the extent of oxygen binding, and autoxidation [29,34,44–46]. The current study on DHP provides insights into a new example obeying the 'sliding scale rule' in a hemeprotein with a very different structural fold, a globin exhibiting multiple enzyme functions. The ratio of $K_D$(NO)/$K_D$(CO) and $K_D$(CO)/$K_D$($O_2$) remains 3-4 orders regardless of the protein fold. The fact that DHP conforms well to the 'sliding scale rule' is consistent with its neutral proximal histidine heme ligand and the results of many experiments, suggesting a large and relatively open-distal pocket in DHP [53,54]. Therefore, the binding of DHP to diatomic gaseous ligands follows single-step binding kinetics with no intermediates, but at the same time the dissociation constant is an order of magnitude larger than those of other typical globins.

## Abbreviations

6cLS, six-coordinated low-spin; CCP, cytochrome *c* peroxidase; DHP, dehaloperoxidase–hemoglobin; FHb, flavohemoglobin; Hb, hemoglobin; H-NOX, heme nitric oxide and oxygen-binding protein; HRP, horseradish peroxidase; Lb, soybean leghemoglobin; Mb, myoglobin; MD, molecular dynamics;

*Ns* H-NOX, H-NOX from *Nostoc* sp. PCC7120; sGC, human soluble guanylyl cyclase; SWMb, sperm whale myoglobin; *Tt* H-NOX, H-NOX from *Thermoanaerobacter tengcongensis*.

### Author Contribution

G.W. performed the experimental work and wrote the manuscript. J.Z. expressed and purified the proteins and revised the manuscript. S.F. and A.-L.T. conceived the study and wrote and revised the manuscript.

### Funding

This work was supported by NIH grant [NS094535] to A.-L.T. and NSF grant [CHE-1507947] to S.F.

### Competing Interests

The Authors declare that there are no competing interests associated with the manuscript.

## References

1 Chen, Y.P., Woodin, S.A., Lincoln, D.E. and Lovell, C.R. (1996) An unusual dehalogenating peroxidase from the marine terebellid polychaete *Amphitrite ornata*. *J. Biol. Chem.* **271**, 4609–4612 doi:10.1074/jbc.271.9.4609
2 Han, K., Woodin, S.A., Lincoln, D.E., Fielman, K.T. and Ely, B. (2001) *Amphitrite ornata*, a marine worm, contains two dehaloperoxidase genes. *Mar. Biotechnol.* **3**, 287–292 doi:10.1007/s10126-001-0003-8
3 Ma, H., Thompson, M.K., Gaff, J. and Franzen, S. (2010) Kinetic analysis of a naturally occurring bioremediation enzyme: dehaloperoxidase-hemoglobin from *Amphitrite ornata*. *J. Phys. Chem. B* **114**, 13823–13829 doi:10.1021/jp1014516
4 Zhao, J., Lu, C. and Franzen, S. (2015) Distinct enzyme–substrate interactions revealed by two dimensional kinetic comparison between dehaloperoxidase-hemoglobin and horseradish peroxidase. *J. Phys. Chem. B* **119**, 12828–12837 doi:10.1021/acs.jpcb.5b07126
5 Franzen, S., Thompson, M.K. and Ghiladi, R.A. (2012) The dehaloperoxidase paradox. *Biochim. Biophys. Acta, Proteins Proteomics* **1824**, 578–588 doi:10.1016/j.bbapap.2011.12.008
6 D'Antonio, J., D'Antonio, E.L., Thompson, M.K., Bowden, E.F., Franzen, S., Smirnova, T. et al. (2010) Spectroscopic and mechanistic investigations of dehaloperoxidase B from *Amphitrite ornata*. *Biochemistry* **49**, 6600–6616 doi:10.1021/bi100407v
7 D'Antonio, E.L., Chen, T.K., Turner, A.H., Santiago-Capeles, L. and Bowden, E.F. (2013) Voltammetry of dehaloperoxidase on self-assembled monolayers: reversible adsorptive immobilization of a globin. *Electrochem. Commun.* **26**, 67–70 doi:10.1016/j.elecom.2012.10.011
8 D'Antonio, E.L., Bowden, E.F. and Franzen, S. (2012) Thin-layer spectroelectrochemistry of the Fe(III)/Fe(II) redox reaction of dehaloperoxidase-hemoglobin. *J. Electroanal. Chem.* **668**, 37–43 doi:10.1016/j.jelechem.2011.12.015
9 Ayala, M. (2010) Redox potential of peroxidases. In *Biocatalysis Based on Heme Peroxidases: Peroxidases as Potential Industrial Biocatalysts* (Torres, E. and Ayala, M., eds), pp. 61–77. Springer, Berlin, Heidelberg
10 D'Antonio, J. and Ghiladi, R.A. (2011) Reactivity of deoxy- and oxyferrous dehaloperoxidase B from *Amphitrite ornata*: identification of compound II and its ferrous–hydroperoxide precursor. *Biochemistry* **50**, 5999–6011 doi:10.1021/bi200311u
11 Chen, Z., de Serrano, V., Betts, L. and Franzen, S. (2009) Distal histidine conformational flexibility in dehaloperoxidase from *Amphitrite ornata*. *Acta Crystal. D Biol. Crystallogr.* **65**, 34–40 doi:10.1107/S0907444908036548
12 Du, J., Huang, X., Sun, S., Wang, C., Lebioda, L. and Dawson, J.H. (2011) *Amphitrite ornata* dehaloperoxidase (DHP): investigations of structural factors that influence the mechanism of halophenol dehalogenation using 'peroxidase-like' myoglobin mutants and 'myoglobin-like' DHP mutants. *Biochemistry* **50**, 8172–8180 doi:10.1021/bi2009129
13 Osborne, R.L., Raner, G.M., Hager, L.P. and Dawson, J.H. (2006) *C. fumago* chloroperoxidase is also a dehaloperoxidase: oxidative dehalogenation of halophenols. *J. Am. Chem. Soc.* **128**, 1036–1037 doi:10.1021/ja056213b
14 Sumithran, S., Sono, M., Raner, G.M. and Dawson, J.H. (2012) Single turnover studies of oxidative halophenol dehalogenation by horseradish peroxidase reveal a mechanism involving two consecutive one electron steps: toward a functional halophenol bioremediation catalyst. *J. Inorg. Biochem.* **117**, 316–321 doi:10.1016/j.jinorgbio.2012.09.017
15 Franzen, S., Belyea, J., Gilvey, L.B., Davis, M.F., Chaudhary, C.E., Sit, T.L. et al. (2006) Proximal cavity, distal histidine, and substrate hydrogen-bonding mutations modulate the activity of *Amphitrite ornata* dehaloperoxidase. *Biochemistry* **45**, 9085–9094 doi:10.1021/bi060020z
16 Nicoletti, F.P., Thompson, M.K., Howes, B.D., Franzen, S. and Smulevich, G. (2010) New insights into the role of distal histidine flexibility in ligand stabilization of dehaloperoxidase–hemoglobin from *Amphitrite ornata*. *Biochemistry* **49**, 1903–1912 doi:10.1021/bi9020567
17 Zhao, J., de Serrano, V., Zhao, J., Le, P. and Franzen, S. (2013) Structural and kinetic study of an internal substrate binding site in dehaloperoxidase-hemoglobin A from *Amphitrite ornata*. *Biochemistry* **52**, 2427–2439 doi:10.1021/bi301307f
18 Du, J., Sono, M. and Dawson, J.H. (2010) Functional switching of *Amphitrite ornata* dehaloperoxidase from $O_2$-binding globin to peroxidase enzyme facilitated by halophenol substrate and $H_2O_2$. *Biochemistry* **49**, 6064–6069 doi:10.1021/bi100741z
19 Sun, S., Sono, M., Du, J. and Dawson, J.H. (2014) Evidence of the direct involvement of the substrate TCP radical in functional switching from oxyferrous $O_2$ carrier to ferric peroxidase in the dual-function hemoglobin/dehaloperoxidase from *Amphitrite ornata*. *Biochemistry* **53**, 4956–4969 doi:10.1021/bi5002757
20 Zhao, J., Zhao, J. and Franzen, S. (2013) The regulatory implications of hydroquinone for the multifunctional enzyme dehaloperoxidase-hemoglobin from *Amphitrite ornata*. *J. Phy. Chem. B* **117**, 14615–14624 doi:10.1021/jp407663n
21 Barrios, D.A., D'Antonio, J., McCombs, N.L., Zhao, J., Franzen, S., Schmidt, A.C. et al. (2014) Peroxygenase and oxidase activities of dehaloperoxidase-hemoglobin from *Amphitrite ornata*. *J. Am. Chem. Soc.* **136**, 7914–7925 doi:10.1021/ja500293c
22 McCombs, N.L., D'Antonio, J., Barrios, D.A., Carey, L.M. and Ghiladi, R.A. (2016) Nonmicrobial nitrophenol degradation via peroxygenase activity of dehaloperoxidase-hemoglobin from *Amphitrite ornata*. *Biochemistry* **55**, 2465–2478 doi:10.1021/acs.biochem.6b00143

Biochemical Journal (2017) **474** 3485–3498
DOI: 10.1042/BCJ20170515


23 Ghiladi, R.A., McCombs, N.L. and Carey, L.M. (2016) The multiple enzymatic activities of the hemoglobin dehaloperoxidase from *Amphitrite Ornata. 19th Conference on Oxygen-binding and Sensing Proteins*, Hamburg, Germany, pp. 58

24 Sun, S., Sono, M., Wang, C., Du, J., Lebioda, L. and Dawson, J.H. (2014) Influence of heme environment structure on dioxygen affinity for the dual function *Amphitrite ornata* hemoglobin/dehaloperoxidase. Insights into the evolutional structure–function adaptations. *Arch. Biochem. Biophys.* **545**, 108–115 doi:10.1016/j.abb.2014.01.010

25 Carver, T.E., Brantley, Jr, R.E., Singleton, E.W., Arduini, R.M., Quillin, M.L., Phillips, Jr, G.N. et al. (1992) A novel site-directed mutant of myoglobin with an unusually high $O_2$ affinity and low autooxidation rate. *J. Biol. Chem.* **267**, 14443–14450 PMID:1629229

26 Draghi, F., Miele, A.E., Travaglini-Allocatelli, C., Vallone, B., Brunori, M., Gibson, Q.H. et al. (2002) Controlling ligand binding in myoglobin by mutagenesis. *J. Biol. Chem.* **277**, 7509–7519 doi:10.1074/jbc.M109206200

27 Quillin, M.L., Li, T., Olson, J.S., Phillips, Jr, G.N., Dou, Y., Ikeda-Saito, M. et al. (1995) Structural and functional effects of apolar mutations of the distal valine in myoglobin. *J. Mol. Biol.* **245**, 416–436 doi:10.1006/jmbi.1994.0034

28 Tsai, A.L., Berka, V., Martin, E. and Olson, J.S. (2012) A 'Sliding-scale rule' for selectivity between NO, CO and $O_2$ by heme protein sensors. *Biochemistry* **51**, 172–186 doi:10.1021/bi2015629

29 Tsai, A.L., Martin, E., Berka, V. and Olson, J.S. (2012) How do heme-protein sensors exclude oxygen? Lessons learned from cytochrome c′, *Nostoc puntiforme* heme nitric oxide/oxygen-binding domain, and soluble guanylyl cyclase. *Antioxid Redox Signal.* **17**, 1246–1263 doi:10.1089/ars.2012.4564

30 Berry, E.A. and Trumpower, B.L. (1987) Simultaneous determination of hemes a, b, and c from pyridine hemochrome spectra. *Anal. Biochem.* **161**, 1–15 doi:10.1016/0003-2697(87)90643-9

31 Capellos, C. and Bielski, B.H.J. (1972) *Kinetic Systems, Mathematical Description of Chemical Kinetics in Solution*. Wiley Interscience, New York

32 Lewis, R.S. and Deen, W.M. (1994) Kinetics of the reaction of nitric oxide with oxygen in aqueous solutions. *Chem. Res. Toxicol.* **7**, 568–574 doi:10.1021/tx00040a013

33 Brent, R.P. (1973) *Algorithms for Minimization Without Derivatives*. Prentice-Hall, Englewood Cliffs, NJ

34 Wu, G., Liu, W., Berka, V. and Tsai, A.L. (2017) Gaseous ligand selectivity of the H-NOX sensor protein from *Shewanella oneidensis* and comparison to those of other bacterial H-NOXs and soluble guanylyl cyclase. *Biochimie* **140**, 82–92 doi:10.1016/j.biochi.2017.06.014

35 Yonetani, H. and Yamamoto, H. (1973) Optical and electron paramagnetic resonance properties of the nitric oxide compounds of cytochrome c peroxidase and horseradish peroxidase. In *Oxidases and Related Redox Systems* (King, T.E., Mason, H.S. and Morrison, M., eds), pp. 279–299. University Park Press, Baltimore, MD

36 Nienhaus, K., Nickel, E., Davis, M.F., Franzen, S. and Nienhaus, G.U. (2008) Determinants of substrate internalization in the distal pocket of dehaloperoxidase hemoglobin of *Amphitrite ornata*. *Biochemistry* **47**, 12985–12994 doi:10.1021/bi801564r

37 Zhao, J., de Serrano, V. and Franzen, S. (2014) A model for the flexibility of the distal histidine in dehaloperoxidase-hemoglobin A based on X-ray crystal structures of the carbon monoxide adduct. *Biochemistry* **53**, 2474–2482 doi:10.1021/bi5001905

38 Feis, A., Lapini, A., Catacchio, B., Brogioni, S., Foggi, P., Chiancone, E. et al. (2008) Unusually strong H-bonding to the heme ligand and fast geminate recombination dynamics of the carbon monoxide complex of *Bacillus subtilis* truncated hemoglobin. *Biochemistry* **47**, 902–910 doi:10.1021/bi701297f

39 Guallar, V., Lu, C., Borrelli, K., Egawa, T. and Yeh, S.-R. (2009) Ligand migration in the truncated hemoglobin-II from *Mycobacterium tuberculosis*: the role of G8 tryptophan. *J. Biol. Chem.* **284**, 3106–3116 doi:10.1074/jbc.M806183200

40 Franzen, S., Roach, M.P., Chen, Y.-P., Dyer, R.B., Woodruff, W.H. and Dawson, J.H. (1998) The unusual reactivities of *Amphitrite ornata* dehaloperoxidase and *Notomastus lobatus* chloroperoxidase do not arise from a histidine imidazolate proximal heme iron ligand. *J. Am. Chem. Soc.* **120**, 4658–4661 doi:10.1021/ja973212d

41 Hoshino, M., Ozawa, K., Seki, H. and Ford, P.C. (1993) Photochemistry of nitric oxide adducts of water-soluble iron(III) porphyrin and ferrihemoproteins studied by nanosecond laser photolysis. *J. Am. Chem. Soc.* **115**, 9568–9575 doi:10.1021/ja00074a023

42 Rose, E.J., Venkatasubramanian, P.N., Swartz, J.C., Jones, R.D., Basolo, F. and Hoffman, B.M. (1982) Carbon monoxide binding kinetics in 'capped' porphyrin compounds. *Proc. Natl Acad. Sci. U.S.A.* **79**, 5742–5745 doi:10.1073/pnas.79.18.5742

43 Tsai, A.L. (1994) How does NO activate hemeproteins? *FEBS Lett.* **341**, 141–145 doi:10.1016/0014-5793(94)80445-1

44 Wu, G., Liu, W., Berka, V. and Tsai, A.L. (2013) The selectivity of *Vibrio cholerae* H-NOX for gaseous ligands follows the 'sliding scale rule' hypothesis. Ligand interactions with both ferrous and ferric *Vc* H-NOX. *Biochemistry* **52**, 9432–9446 doi:10.1021/bi401408x

45 Wu, G., Liu, W., Berka, V. and Tsai, A.L. (2015) H-NOX from *Clostridium botulinum*, like H-NOX from *Thermoanaerobacter tengcongensis*, binds oxygen but with a less stable oxyferrous heme intermediate, *Biochemistry* **54**, 7098–7109 doi:10.1021/acs.biochem.5b00994

46 Tsai, A.L., Berka, V., Martin, F., Ma, X., van den Akker, F., Fabian, M. et al. (2010) Is *Nostoc* H-NOX a NO sensor or redox switch? *Biochemistry* **49**, 6587–6599 doi:10.1021/bi1002234

47 Poulos, T.L. (2014) Heme enzyme structure and function. *Chem. Rev.* **114**, 3919–3962 doi:10.1021/cr400415k

48 Zhao, J., de Serrano, V., Dumarieh, R., Thompson, M., Ghiladi, R.A. and Franzen, S. (2012) The role of the distal histidine in $H_2O_2$ activation and heme protection in both peroxidase and globin functions. *J. Phys. Chem. B* **116**, 12065–12077 doi:10.1021/jp300014b

49 Dou, Y., Maillett, D.H., Eich, R.F. and Olson, J.S. (2002) Myoglobin as a model system for designing heme protein based blood substitutes. *Biophys. Chem.* **98**, 127–148 doi:10.1016/S0301-4622(02)00090-X

50 Eich, R.F. (1997) *Reactions of Nitric Oxide with Myoglobin*. Biochemistry and Cell Biology, Rice University, Houston

51 Foley, E.W. (2005) *Physiologically Relevant Reactions of Myoglobin and Hemoglobin with NO*. Biochemistry and Cell Biology, Rice University, Houston

52 Tsai, A.L. and Kulmacz, R.J. (2010) Prostaglandin H synthase: resolved and unresolved mechanistic issues. *Arch. Biochem. Biophys.* **493**, 103–124 doi:10.1016/j.abb.2009.08.019

53 Zhao, J., Moretto, J., Le, P. and Franzen, S. (2015) Measurement of internal substrate binding in dehaloperoxidase–hemoglobin by competition with the heme–fluoride binding equilibrium. *J. Phys. Chem. B* **119**, 2827–2838 doi:10.1021/jp512996v

54 de Serrano, V. and Franzen, S. (2012) Structural evidence for stabilization of inhibitor binding by a protein cavity in the dehaloperoxidase-hemoglobin from *Amphitrite ornata*. *Peptide Sci.* **98**, 27–35 doi:10.1002/bip.21674